A LIGHTWEIGHT, COST-EFFICIENT, SOLID-STATE LIDAR SYSTEM UTILIZING LIQUID CRYSTAL TECHNOLOGY FOR LASER BEAM STEERING FOR ADVANCED DRIVER ASSISTANCE

Ben Luey
Scott R. Davis
Scott D. Rommel
Derek Gann
Joseph Gamble
Michael Ziemkiewicz
Mike Anderson
Roxie Paine
Analog Devices, Inc.
USA

Paper Number 17-0323

ABSTRACT

LiDAR is an instrumental component of the sensor fusion system required for advanced collision avoidance, automatic emergency braking, and autonomous driving. This conference proceeding describes a solid-state LiDAR system that utilizes liquid crystal technology to closely replicate the human driver's eyes without blind spots. The electro-optic (EO) beam steerer operates with a laser wavelength around 1550 nm, which enables high intensity light pulses while maintaining eye-safety. This system provides continuous scanning at 0.1° angular resolution at long range. Unlike other technologies, this technique is purely refractive. It can employ foveated vision, and thus closely mimic the human eye. It can utilize "track and hold" onto one or more distinct moving objects and can dynamically adjust what objects to track in addition to how big a scene to take at low resolution and what area(s) to take at high resolution. This flexibility enables the laser to scan in a pattern that maximizes the utility of the information. Our first proof of concept demonstration has range beyond 200m and a dynamic field-of-view (FOV) up to 20° x 2.5°.

INTRODUCTION & OVERVIEW

In this paper we will present the design and performance of a fully non-mechanical, real-time, solid-state LiDAR system. This approach provides a path for excellent LiDAR performance in a small system box that can be mounted on a vehicle in production. This electro-optic (EO) or solid-state LiDAR system operates at eye-safe wavelengths, provides dynamic control over the entire field-of-view (FOV), has no blind-spots and a path for cost reduction in volume. These advantages are enabled by the non-mechanical beam steerer that uses our patented Liquid Crystal (LC) Waveguide technology to continuously tune optical refraction, providing high-speed, continuous, wide-angle, non-mechanical beamsteering. The elimination of all moving parts provides significant benefits: i) enhanced functionality (dynamic frame sizes), ii) vibration immunity, iii) no mechanical wear and tear, and ultimately iv) reduced total cost of ownership when compared to typical mechanical approaches. Moreover, unlike many non-mechanical approaches, this technology has no blind-spots and high optical efficiency. The primary application for this novel LiDAR system is advanced driver assistance systems (ADAS) and autonomous vehicles that need cost-effective, mechanically robust, high-resolution LiDAR. Table 1 summarizes the performance of this first generation prototype.

In the remainder of this paper we will briefly describe our beamsteerer technology and how it is fundamentally different from other approaches. We will then explain how the scanner was integrated into an EO-scanned solid-state LiDAR system and show the performance of this LiDAR system.

Table 1.
Performance capabilities for the EO scanned LiDAR system

Attribute	Prototype System Performance
Size	3,500 cm^3
Power Consumption	< 20 Watts
FOV	20° x 2.5°
Steering Precision	< 0.01°
Range Accuracy[B]	<10 cm
Range for 10% reflector	110m
Maximum Range	>200 m
Laser Pulse Energy	~1μJ
Laser Rep Rate	25 kHz
Max LiDAR Frame Size	300 × 50
LiDAR Frame Rate	1 Hz (variable, dependent on frame size)
Laser Wavelength	1550 nm
Dynamic / Foveated FOV	Yes
Point and Hold Possible	Yes
Solid State / No Moving Parts	Yes

NEW ELECTRO-OPTIC LASER SCANNERS: CIRCUMVENTING THE SIZE, WEIGHT, AND POWER LIMITATIONS OF MECHANICS

Replacing Mechanics: The Long-Standing Dream
EO scanners that provide continuous coverage over wide-angles and can provide high-speed controlled-sweeps over thousands of spots, all in a compact and simple package simply do not exist. Numerous past attempts have yielded wide-angle but discrete-step binary[1-3] and ternary[4, 5] angle-switches, but these all require a fine steering element to fill-in the large gaps between the discrete angles (>90% of FOV not addressed). For the past several decades people have worked primarily on tunable diffraction grating approaches, with most of the effort focused on thermal-optical or liquid crystal (LC) optical phased arrays (OPAs)[6-8], but also with efforts on MEMs arrays,[9, 10] electro-wetting arrays,[11] and acousto-optics. Despite significant advances, some inherent limitations with diffractive approaches remain. Diffractive approaches are not continuous and have blind spots in their steering unless their steering range is significantly reduced. Beam quality, optical insertion loss and side-lobes can also be a challenge. Finally, the moving locations of 2pi resets in OPAs typically make it impossible to scan in an analog or continuous fashion. Discrete or quantized scanning requires stepping through each intermediate spot and waiting for the system to stabilize on that point before going to the next one. This makes that total scan time scale linearly with the number of points to be scanned. In the case of an LC OPA, an LC relaxation (5 - 30 ms) must occur for each point. Therefore, to do a linear spot-to-spot sweep or scan across a 1000 spot FOV, i.e., 1000 steps, one must wait between 5-30 seconds. A 1000 × 100 raster scan would take between 8 to 25 minutes! Switch times on the order of microseconds are necessary for diffractive approaches to realize reasonable frame rates. Si waveguide OPAs show promise of reduced switching times, but thermal-optic tuning also presents a challenge for power consumption and performance over temperature as tight integration makes it hard to thermally isolate each switch element. What is needed is a high-speed, non-diffractive, large-angle continuous scanner. Unfortunately all prior refractive scanning attempts

only realize a small voltage control over optical phase, which means only a small scan angle and/or aperture.[12-15] For example, the KTN scanner from NTT used 250V and only realized 20 spots with a 300 micron wide beam.[14]

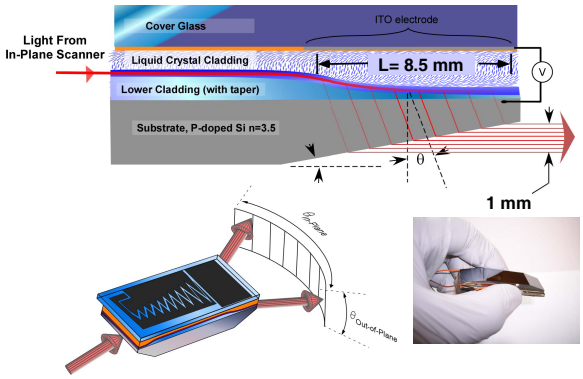

Figure 1. TOP) The basic design of a liquid crystal (LC) waveguide with a steerable output coupler. BOTTOM LEFT) LC waveguide with patterned ITO electrodes to give in-plane beamsteering. BOTTOM RIGHT) A finished 2D beamsteerer that can steer a 1mm beam 30° x 5°.

We circumvent these prior limitations by using our proprietary **S**teerable **E**lectro **E**vanescent **O**ptical **R**efractor (SEEOR). The underlying photonic architecture utilizes a liquid crystal (LC) material as a cladding layer in a slab waveguide to generate large refractive index changes of up to Δn_{eff} =0.04 for the guided wave (Figure 1, top). The evanescent field of the fundamental waveguide mode interacts with the LC layer near the surface of the waveguide where the LC molecules are well-ordered and experience high restoring forces. LC waveguides can exhibit losses under 0.5 dB/cm and have sub-millisecond response times. The liquid crystal layer is held in place by a cover glass as in standard liquid crystal displays (LCDs). This architecture decouples the interaction length from the thickness of the LC layer, enabling unprecedented analog voltage control over optical phase (>2 mm tuning over optical phase has been demonstrated), with fast response times and low losses.

The top of Figure 1 shows the structure for vertical or out-of-plane beamsteering. This is achieved by allowing the evanescent field to contact and tunnel into a high-index silicon substrate by tapering the silica subcladding. A simple S-taper results in a Gaussian beam output with $M^2 \sim 1$. The out coupling angle θ into the silicon substrate is given by

$$\sin\theta = \frac{n_{eff}}{n_{silicon}}, \qquad (1)$$

where n_{eff} is the index of the guided wave and depends on the index of the core, subcladding, and the voltage-dependent index of the LC layer. The output beam exits the waveguide facet near Brewster's angle. Note that the steering in air is much larger than steering inside silicon because of the index difference and anamorphic compression at the facet. Devices that steer a 0.2° diverging beam over 15° have been demonstrated.

In-plane beamsteering is achieved by patterning the coverplate electrode into a succession of prisms. The LC waveguide enables the index under the prism to be tuned leading to tunable refraction. By increasing the width of the prisms along the propagation direction, the sweep of the beam can be accommodated leading to a "shape optimized" steering electrode as shown in the bottom left of Figure 1. Both right and left steering electrodes can be used to double the in-plane steering range.

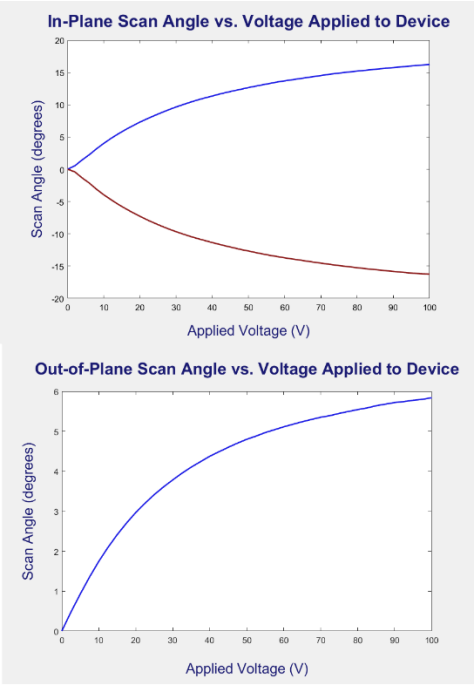

Figure 2. Plot of EO scan angle as a function of waveguide voltage for a SEEOR.

Figure 2 shows the SEEOR scan angle vs voltage. Because the tuning is controlled by an analog voltage, the tuning is fundamentally continuous. In addition to having no blind spots, when jumping between two angles, the beam steerer must scan

through every angle between the start and stop angles. We have built SEEOR chips that continuously scan up to 30°×5°. In other devices, we have also demonstrated: i) 270° of 1-D steering; ii) high speed (1 spot per us); and iii) large aperture (1.2 cm) scanning. SEEOR's are compact (~6 cm^3), low power (only milliWatts), and simple (only 3 electrodes).

The SEEOR chips already provide an unprecedented level of EO beamsteering. That said, these chips are a new technology and constantly being improved. Efforts to increase the FOV and / or beamsize are ongoing.

Utilizing SEEORs for a Solid-State LiDAR Device
We utilize a discretely scanned staring sensor to receive the reflected LiDAR pulses. This bi-static approach is the most common detection method among LiDAR manufacturers. In a typical non-scanned system, the imaged spot just fills the detector area to minimize detection of background light. For our EO-scanned launch beam this presents a problem because the spot will sweep across the detector. Our answer is to use low capacitance InGaAs to enable a larger detector area while keeping the detector capacitance low. In this configuration the active area of the detector is necessarily larger than that for a non-steered beam. Having a larger detector has numerous disadvantages: increased detector capacitance, which decreases bandwidth and increases electronics noise; increased detector dark current; increased background radiation from the larger FOV. We minimize all these effects by using an array sensor that is segmented. (see Figure 3 for conceptual diagram). In this way the capacitance, dark current and background light is reduced by the number of segments in the array. The FOV of the segmented return-array is adjusted synchronously with the scanner so the receive FOV includes the scanner's field-of-illumination, as shown in Figure 3.

This approach provides an excellent trade-off between scanned LiDAR and a flash approach. The spatial resolution of flash LiDAR is given by the diode array size and all diodes must be illuminated simultaneously. With our scanned LiDAR the spatial resolution is giving by the scanner resolution and the detector elements are sequentially illuminated so that one timing circuit can be sequentially switched onto each detector element. This flying-spot LiDAR scanner can have reduced cost and require less optical power when compared to a purely flash approach. This approach also adds flexibility; it can provide a dynamic FOV, point-and-hold tracking, low density/high speed frames, and much more. We believe this architecture provides the best combination of performance attributes: fully non-mechanical, wide FOV, amenable to a low SWaP laser, and overall system simplicity.

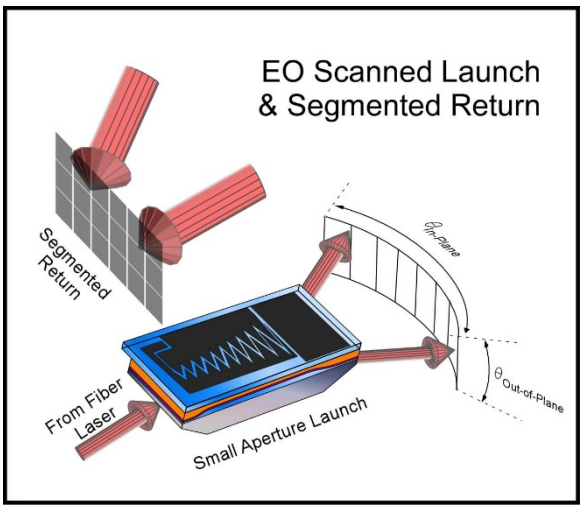

Figure 3. Schematic of the EO scanner LiDAR architecture. A laser pulse is launched through the EO scanner and the return light is received through a synchronized discrete scanning stage onto a segmented array.

SOLID-STATE LIDAR PROTOTYPE & DEMONSTRATION

Prototype Assembly and Components
We placed lens with a 45mm clear aperture and 40mm focal length in front of the detector. For our detector geometry, this produced a FOV of 20° x 2.5°. Although the SEEOR can scan wider, the LiDAR FOV was limited by the detector geometry and the focal length of the lens. The receive FOV can be increased in a variety of manners by utilizing: i) a more complex receive optic; ii) a larger detector; iii) multiple detectors; iv) a faster but smaller receive optic; v) or some combination of these changes.

To measure the time-of-flight (TOF) of the laser pulse, the output of the PIN photodiode goes into a trans-impedance amplifier and then a threshold comparator. The timing on digital output of the comparator is then measured using a direct TOF technique. This technique calculates the time from the initial launch of the flash pulse (measured with the flash detector) to both the leading and falling edge of the return light pulse. The time between the rising and falling edge is an indication of the intensity of the received light pulse. Our implementation was only sensitive to the first return of the light pulse. Future work will improve the sensitivity of these

electronics and will not be limited to only the first return of the light pulse.

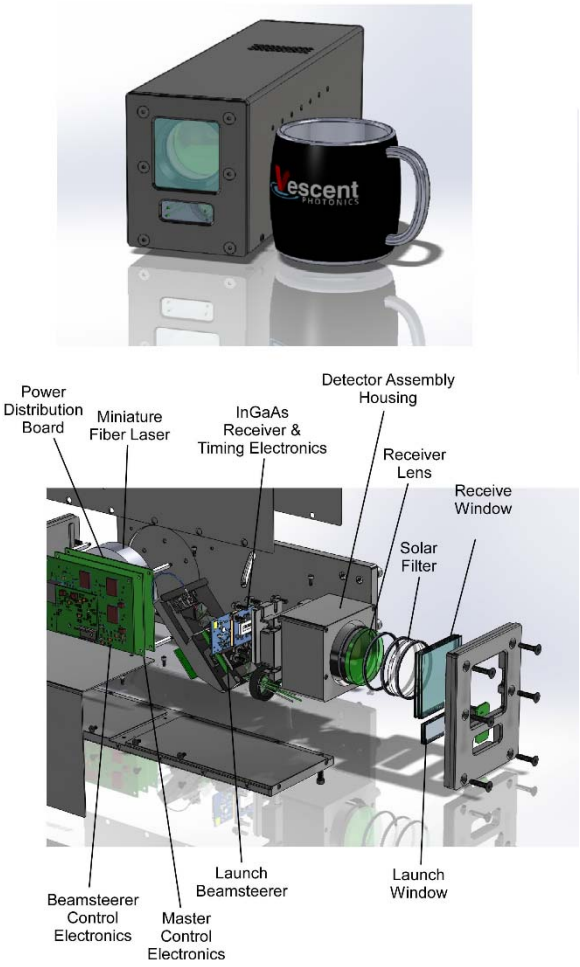

Figure 4. TOP) Solid module for full LiDAR system. BOTTOM) Blown-up solid model for the EO scanned LiDAR unit with some key components identified.

Figure 4, Figure 5, and Figure 7 show details of the first generation EO scanned LiDAR system. This system was not optimized for size and significant reductions are planned in future designs. Figure 4 shows details of the package interior with important components identified. The launch aperture is below the receive aperture, and quite a bit smaller. A compact fiber laser is coupled to the SEEOR beamsteerer. This scanner is mounted in a way that allows adjustment to the exit angle to align it with the exit aperture. Once the beam leaves the scanner it can be EO steered over the full LiDAR FOV of 20° × 2.5°. The return light first passes through a solar filter and then hits the 50 mm diameter receive optic. Figure 5 shows a detailed view of the receiver housing. This housing is designed to be light tight to prevent false triggers to the timing electronics. A flash detector (hard to see in the pictures) detects the zero time of the laser pulse prior to entry into the SEEOR beamsteerer. The receiver housing allows adjustment between the receiver lens and the InGaAs array. This is aligned so that the focal depth of the lens is just in-front of the array. In this way, aberrations are evenly distributed across the array. This can be done because the angular position is determined not by the array but by the beamsteerer.

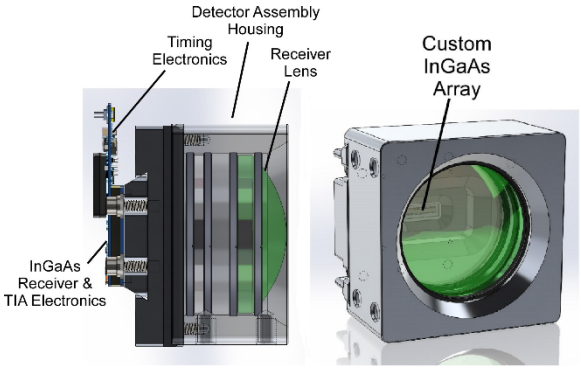

Figure 5. Solid model of the detector housing assembly. This unit is designed to be light tight to prevent unwanted returns.

Figure 6. Fully assembled LiDAR system.

The electronics inside the unit include the beamsteerer driver board, with a SEEOR temp control daughter board, a power distribution board, and the master control board or "brain board" that handles the computer interface. The high-speed timing electronics are mounted directly behind the InGaAs array and communicate with the brain board via a digital interface. The fiber laser is mounted directly to a metal support wall, which serves as a heat sink for the laser.

A picture of the first generation device, as it is being assembled, is shown in Figure 7. This first unit was not designed to minimize size, but rather as a proof-of-concept unit. Most of the volume is for electronics, which can be put on an ASIC, and would significantly reduce size and cost. The fully assembled LiDAR system can be seen in Figure 6.

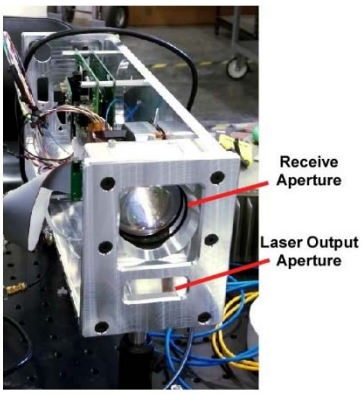

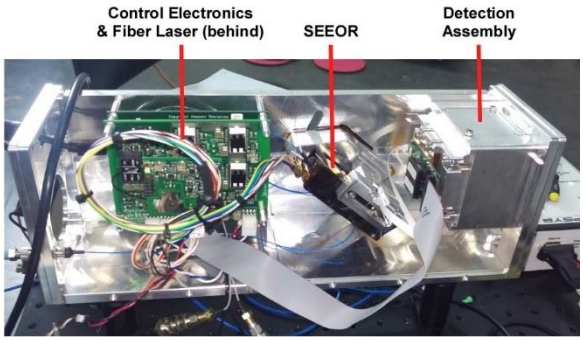

Figure 7. TOP) Top view of the first generation solid-state LiDAR unit while under construction. As can be seen, much of the volume is electronics (which can be significantly reduced) and empty space. BOTTOM) Side view of the same.

LiDAR Images taken with LiDAR System

The left side Figure 8 shows the LiDAR unit set to point down a hallway that is approximately 100 feet long. The upper right and bottom of Figure 8 shows two different perspectives of the acquired point cloud. No imaging processing, averaging or filtering was done to these or any other LiDAR images shown in this paper. Figure 9 and Figure 10 show similar images for different scenes.

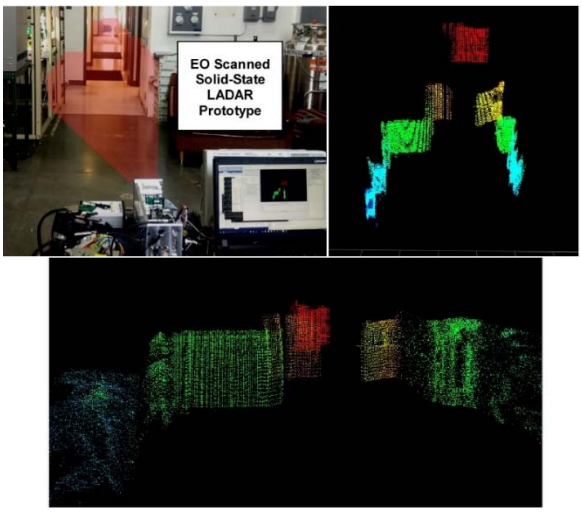

Figure 8. UPPER LEFT) Picture of the prototype as it is aimed to image down a hallway. The transparent red area approximately shows the imaged scene. UPPER RIGHT and BOTTOM) Different perspectives of point-cloud generated from a single shot.

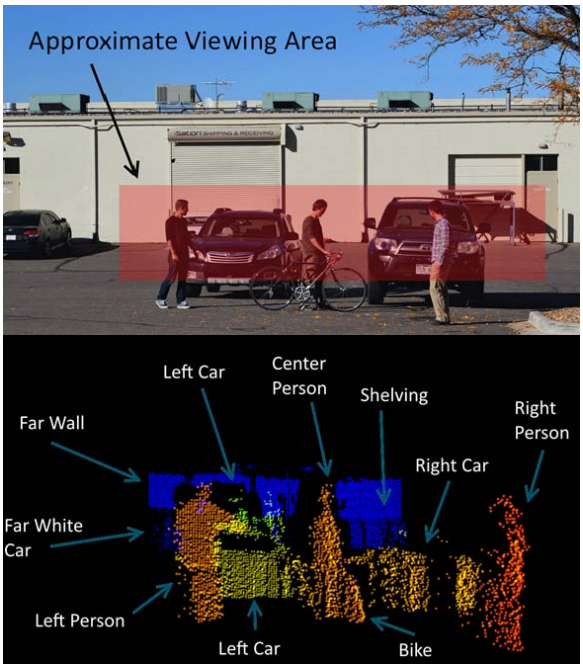

Figure 9. TOP) Target scene including two cars, three people and a bicycle. BOTTOM) LiDAR image of the same scene. Point-cloud data is rotated slightly to show depth.

Figure 10. TOP) Target scene with a large wall 180 ft away. Far back wall is 285ft away. BOTTOM) LiDAR image of the same scene. Dark blue is the far wall and the light blue are the AC units mounted on the roof approximately 225ft away.

LiDAR Data

Two equivalent units were built and their performance was characterized using two NIST-calibrated targets (14% and 28% reflectivity) and a variety of other targets that were calibrated relative to the NIST-calibrated targets. Both units had similar performance and were able to range 10% targets out passed 100m with a 1uJ output laser pulse. A target that was 40% reflective could range out to 220m. The width of the returned light pulse is an indication of how much light was received and can be used as a signal strength metric. A plot of the light pulse width (called measured intensity) vs distance for various targets is shown below in Figure 11. At further distances, the returned pulse width gets smaller as the signal gets weaker and we empirically determined a noise floor where we could no longer consistently (>95% of the time) see targets. The curves in Figure 11 can be used to estimate SNR for different target reflectivities and distances. No averaging or other post-processing was applied to this data.

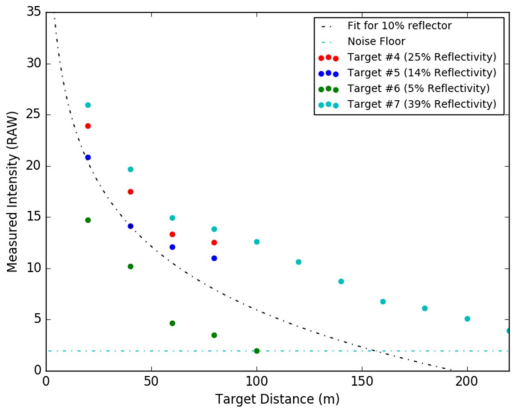

Figure 11. Uncalibrated Measured intensity as measured by pulse width is plotted vs target distance for various targets. The SNR is scales with the measured intensity, so this plot can be used to calculate the SNR for various target reflectivities and distances. An empirically measured noise floor set the weakest intensity signal that could consistently be detected.

While non-linear, the pulse width can be used to calibrate both the measured distance (without calibration, weak signals appear further away than they are) and the reflectivity of the target. While we have not yet done the calibration of target reflectivity, using raw intensity data is still very useful for object detection and perception.

Future LiDAR Improvements

Numerous improvements can be made to this LiDAR system. Currently, our electronics do not support driving the LC in a continuous fashion from minimum to maximum steering. Instead we go to a specific voltage (angle), wait and take data for that LiDAR pulse and then move to the next voltage. This pattern of set, wait, acquire, repeat is much slower than having the LC sweep across the desired FOV. We have previously demonstrated sweeps like this that can scan one resolvable spot per µs. Updated electronics should enable us to get frame rates that are limited by the laser repetition rate rather than the LC, which currently limits our frame rate. Upgraded electronics will also be capable of detecting multiple return pulses per laser pulse. This can be useful for seeing through car windshields and the like or seeing through partially obstructing objects.

Better receive optics should enable a larger FOV without sacrificing range. Further improvements in the analog front-end sensitivity should expand the range further. New designs for the LC waveguide will enable larger steering. Changing the aspect ratio of the detector would enable a better match to the

beamsteerer and increase the FOV of the LiDAR system.

We are investigating laser sources other than a fiber laser. This could drastically decrease the size, weight and power of the LiDAR system and allow a faster laser repetition rate. Moving the electronics into an ASIC would also considerably shrink the system as the laser and the electronics are currently the biggest components in the system. We are also exploring other detector technologoies besides InGaAs.

CONCLUSIONS

We demonstrated the feasibility of utilizing novel electro-evanescent refractive beamsteerers to build an EO scanned LiDAR unit with no-moving parts. The LC waveguide technology and its application to LiDAR is protected by various patents and patent-pending applications[16]. Future versions will have dramatically reduced size, power consumption and a larger FOV. We believe this LiDAR performance is ideal for enabling ADAS and automotive vehicle solutions that need long-range, high-resolution, mechanically-robust LiDAR. We believe this technology can scale to high-volume manufacturing and provide car manufactures a key sensor for enhancing vehicle safety.

ACKNOWLEDGMENTS

The authors wish to thank Todd Meyrath at Vorpal Research for help with the timing electronics, and Jason Auxier and Myron Pauli at Naval Research Labs for useful discussions on EO beamsteering and financial support. This research has been funded in part by NASA phase II SBIR NNX14CG13C.

REFERENCES

[1] Kahn, S. A., and Riza, N. A., "Demonstration of 3-dimensional wide angle laser beam scanner using liquid crystals," Optics Express **12,** 868-882 (2004).

[2] Meyer, H., Riekmann, D., Schmidt, K. P., Schmidt, U. J., Rahlff, M., Schroder, E., and Thrust, W., "Design and performance of a 20-stage digital light beam deflector," Applied Optics **11,** 1932-1936 (1972).

[3] Schmidt, U., and Hust, W., "Optical deflection system including an alternating sequence of birefringent prisms and polarizers," U.S. Patent 3,572,895**,** (1986).

[4] Kim, J., Oh, C., Escuti, M. J., Hosting, L., and Serati, S. A., "Wide-angle, nonmechanical beam steering using thin liquid crystal polarization gratings," in *Advanced Wavefront Control: Methods, Devices, and Applications VI*, (SPIE, 2008), pp. 709302-709301.

[5] Kim, J., Oh, C., Serati, S. A., and Escuti, M. J., "Wide-angle, nonmechanical beam steering with high throughput utilizing polarization gratings," Applied Optics **50,** 2636 (2011).

[6] Borel, J., Deutch, J.-C., Labrunie, G., and Robert, J., "Liquid Crystal Diffraction Grating," U. S. P. Office, ed. (Commissariat A L'Energie Atomique, 1974).

[7] Huignard, J. P., Malard, M., and Corlieu, G. d., "Static Deflector Device for An Infrared Beam," U. S. P. a. T. Office, ed. (Thomson-CSF, USA, 1987).

[8] McManamon, P., Bos, P. J., Escuti, M. J., Heikenfeld, J., Serati, S. A., Xie, H., and Watson, E. A., "A Review of Phased Array Steering for Narrow-Band Electrooptical Systems," Proceedings of the IEEE **97,** 1078-1096 (2009).

[9] Krishnamoorthy, K., Li, K., Yu, D., Lee, D., Heritage, J. P., and Solgaard, O., "Dual mode micromirrors for optical phased array applications," Sensors and Actuators A **A97-98,** (2002).

[10] Ryf, R., Stuard, H. R., and Giles, C. R., "MEMS tip/tilt & piston mirror arrays as diffractive optical elements," Proceeding of SPIE, Bellingham, WA **5894,** 58940C-58941-58911 (2005).

[11] Smith, N. R., Abeysinghe, D. C., Haus, J. W., and Heikenfeld, J., "Agile wide-angle beam steering with electrowetting microprisms," Optics Express **14,** 6557-6563 (2006).

[12] Chiu, Y., Burton, R. S., Stancil, D. D., and Schlesinger, T. E., "Design and Simulation of Waveguide Electrooptic Beam Deflectors," Journal of Lightwave Technology **13,** 2049 (1995).

[13] Chiu, Y., Zou, J., Stancil, D. D., and Schlesinger, T. E., "Shape-Optimized electrooptic beam scanners: Analysis, design, and simulation," Journal of Lightwave Technology **17,** 108 (1999).

[14] Nakamura, K., Miyazu, J., Sasaki, Y., Imai, T., Sasaura, M., and Fujiura, K., "Space-charge-controlled electro-optic effect: Optical beam deflection by electro-optic effect and space-charge-controlled electrical conduction," Journal of Applied Physics **104,** 013105-013101 (2008).

[15] Scrymgeour, D. A., Barad, Y., Gopalan, V., Gahagan, K. T., Jia, Q., Mitchell, T. E., and Robinson, J. M., "Large-angle electro-optic laser scanner on LiTaO3 fabricated by in situ monitoring of ferroelectric-domain micropatterning," Applied Optics **40,** 6236 (2001).

[16] A partial list of patents protecting the LC Waveguide technology, the SEEOR, and their application to LiDAR include patents #9366938, #8989523, #7742664, #8860897, #8380025 and #8311372.